JACS
JOURNAL OF THE AMERICAN CHEMICAL SOCIETY

ARTICLE

pubs.acs.org/JACS

Ultrastable, Redispersible, Small, and Highly Organomodified Mesoporous Silica Nanotherapeutics

Yu-Shen Lin, Nardine Abadeer, Katie R. Hurley, and Christy L. Haynes*

Department of Chemistry, University of Minnesota, Minneapolis, Minnesota 55455, United States

Supporting Information

ABSTRACT: Practical biomedical application of mesoporous silica nanoparticles is limited by poor particle dispersity and stability due to serious irreversible aggregation in biological media. To solve this problem, hydrothermally treated mesoporous silica nanoparticles of small size with dual-organosilane (hydrophilic and hydrophobic silane) surface modification have been synthesized. These highly organomodified mesoporous silica nanoparticles were characterized by transmission electron microscopy, X-ray diffraction, N_2 adsorption−desorption, dynamic light scattering, zeta potential, and solid-state ^{29}Si NMR, and they prove to be very stable in simulated body fluid at physiological temperature. Additionally, they can be dried to a powdered solid and easily redispersed in biological media, maintaining their small size for a period of at least 15 days. Furthermore, this preparation method can be expanded to synthesize redispersible fluorescent and magnetic mesoporous silica nanoparticles. The highly stable and redispersible mesoporous silica NPs show minimal toxicity during in vitro cellular assays. Most importantly, two types of doxorubicin, water-soluble doxorubicin and poorly water-soluble doxorubicin, can be loaded into these highly stable mesoporous silica nanoparticles, and these drug-loaded nanoparticles can also be well-redispersed in aqueous solution. Enhanced cytotoxicity to cervical cancer (HeLa) cells was found upon treatment with water-soluble doxorubicin-loaded nanoparticles compared to free water-soluble doxorubicin. These results suggest that highly stable, redispersible, and small mesoporous silica nanoparticles are promising agents for in vivo biomedical applications.

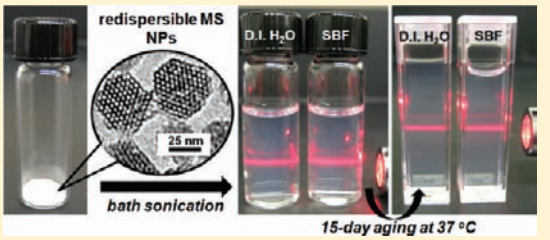

INTRODUCTION

Providing an early and accurate diagnosis of disease and subsequent efficient treatment is a major aim in medicine, and nanotechnology has the potential to advance this goal. In the past decade, great strides have been made in nanomedicine because of the rapid development of nanomaterials. One specific area where nanoscale materials are poised to have an impact is in the targeted use of nanoparticles in tumors, to help physicians perform diagnostics, imaging, and drug delivery.[1,2] Chemotherapeutic drugs are well-known for their adverse side effects such as fatigue, nausea, and hair loss, which result from the way they work to kill quickly dividing cells in the body rather than cancerous cells specifically. Therefore, targeted drug delivery with controlled drug release is a more desirable route in cancer therapy to reduce these negative effects to healthy cells. Mesoporous silica nanoparticles (MS NPs) are small, discrete particles with regularly spaced pores. They are particularly promising for medicine because of their large surface area and pore volume, making them an excellent candidate for drug storage and delivery.[3−5]

Although there is significant literature precedent for the synthesis and biomedical applications of MS NPs, there are several critical issues that result in limited use of these MS NPs in vitro or in vivo. For example, large particle size (>100-nm-diameter) and poor particle stability (aggregation) result in rapid uptake by the reticuloendothelial system (RES).[6−8] Another major hurdle is the possible unintentional toxicity of such MS NPs.[9,10] If the designed NPs cause unintentional damage to benign cells or healthy tissues and organs, their use will be greatly limited in therapeutic applications. Prior to in vivo animal experiments, unintentional cytotoxicity must be minimized. On the basis of the critical considerations described above, a MS NP should possess the following characteristics: (1) small hydrodynamic size (<100 nm); (2) high drug loading capacity; (3) high stability; and (4) minimal unintentional cytotoxicity. Recently, most MS NP work has focused on the development of controlled release using novel methods such as chemical-[11,12] or enzyme-cleavable bonding,[13,14] pH-responsive linkers,[15] or acid-dissolvable ZnO NP[16] and CaP coating[17] as capping agents. However, dispersity of the developed nanoparticles was not carefully examined for any of these controlled drug release MS NPs. Although these precedents successfully demonstrated that a drug can be released in a controlled manner, the most important requirement of using nanotherapeutics for in vivo cancer therapy is having a small hydrodynamic size (<100 nm) in aqueous conditions. Even particles that are small initially will be taken up by the RES if they aggregate upon exposure to biological media, limiting the NP therapeutic efficacy. Additionally, to facilitate clinic use and storage of MS nanotherapetics, it is essential to develop a synthetic method to prepare redispersible MS

Received: September 10, 2011
Published: November 03, 2011

nanotherapetics, those that may be dried and resuspended later with no change in hydrodynamic size or therapeutic efficacy. To date, only a few reports[18−23] have demonstrated that the dispersity of MS NPs can be improved by coating the MS NP surface with a phosphonate,[18] phospholipid,[19] or polyethyleneimine−polyethylene glycol copolymer.[20] However, the hydrodynamic sizes of these phosphate-, phospholipid-, or copolymer-functionalized MS NPs were not carefully examined or are known to be larger than 100 nm in buffered saline solutions. In very recent work, Urata et al. synthesized small MS NPs (∼20 nm) with an ethenylene-bridged silsesquioxane framework using bis(triethoxysily)ethylene precursors.[21] Although this ethenylene-bridged MS NP showed high resistance to biodegradation, no hydrodynamic size data in highly salted solution were demonstrated to prove the colloidal dispersity and long-term stability. Another recent work reported by Cauda et al. developed a "liquid-phase calcination" method to remove surfactant in high-boiling solvents at high temperatures, preventing formation of irreversible NP aggregations.[22] The high temperature calcination in liquid-phase further increased the condensation within the silica network and, accordingly, the stability of the MS NPs. However, the hydrodynamic size of these liquid-phase calcined MS NPs was only measured in ethanol; again, no particle stability data were demonstrated in biological media at physiological temperature. To date, only our previous work showed that sub-50 nm MS NPs (hydrodynamic size <100 nm) with a short-chain polyethylene glycol (PEG) surface modification and hydrothermal treatment exhibited enhanced long-term stability in buffer solutions and cell culture media at physiological temperature as compared to unmodified NPs and PEGylated NPs without hydrothermal treatment.[23] However, no previous work has demonstrated or carefully evaluated MS NP redispersity in water or biological media. Herein, MS NPs were simultaneously functionalized with two types of organosilane (hydrophilic silane and hydrophobic silane) using a hydrothermal treatment. The purpose of modification with both hydrophilic and hydrophobic silanes is to increase aqueous dispersity (using the hydrophilic silane) and reduce silica hydrolysis (using the hydrophobic silane) of MS NPs in aqueous solutions. These highly organomodified MS NPs were thoroughly characterized, and their long-term particle stability in biological media as well as their redispersity were examined by dynamic light scattering. The compatibility of the highly organomodified MS NPs with human endothelial cells, skin fibroblasts, red blood cells, and platelets was assessed. The versatility of this synthetic method was demonstrated by the preparation of redispersible fluorescent and magnetic MS NPs. Furthermore, the water-soluble doxorubicin and a poorly water-soluble version of doxorubicin were loaded into the highly organomodified MS NPs, and their redispersity was also examined by dynamic light scattering. The in vitro therapeutic efficacy of these redispersible doxorubicin-loaded MS NPs on HeLa cancer cells was further evaluated by a traditional cell viability assay. This is the first work successfully synthesizing a small, ultrastable, and redispersible MS nanotherapeutic.

EXPERIMENTAL SECTION

Chemicals and Reagents. All chemicals were used without further purification. Tetraethyl orthosilicate (TEOS), *n*-cetyltrimethylammonium bromide (CTAB), dimethyl sulfoxide (DMSO), trimethylchlorosilane (TMS), fluorescein isothiocyanate (FITC), and polyvinyl pyrrolidone (PVP, average MW 10 000) were purchased from Sigma-Aldrich (Milwaukee, WI). 2-[Methoxy(polyethyleneoxy)propyl]-trimethoxysilane, (PEG-silane, MW 596−725 g/mol, 9−12 EO), and 3,3,3-trifluoropropyldimethylchlorosilane (TFS) were obtained from Gelest (Morrisville, PA). Absolute anhydrous 99.5% ethanol and 95% ethanol were purchased from Pharmco-Aaper (Brookfield, CT). Ultrapure deionized (DI) water was generated using a Millipore Milli-Q system (Billerica, MA). Ammonium hydroxide (NH_4OH, 28−30 wt % as NH_3) and sodium hydroxide (NaOH) were obtained from Mallinckrodt (Phillipsburg, NJ). Acetic acid was obtained from BDH (West Chester, PA). 10× Calcium- and magnesium-free Dulbecco's phosphate-buffered saline (PBS), heat-inactivated fetal bovine serum (FBS), trypsin in 1 mM ethylenediamine tetraacetic acid (EDTA), penicillin streptomycin (PS), and 3-(4,5-dimethylthiazol-2-yl)-2,5-diphenyltetrazolium bromide (MTT) were obtained from Gibco/Invitrogen (Grand Island, NY). High glucose Dulbecco's Modified Eagle's Medium (DMEM) and Minimum Essential Medium Eagle (MEM) were purchased from Hyclone (Logan, UT). Simulated body fluid (SBF) was prepared according to a reported protocol developed by Kokubo et al.[24] Doxorubicin hydrochloride salt was purchased from LC Laboratories (Woburn, MA).

Mesoporous Silica (MS) Nanoparticle (NP) Fabrication. *Unmodified MS NPs (MS42-d) and PEGylated MS NPs without Hydrothermal Treatment (MS42@PEG-c) and with Hydrothermal Treatment (MS42@PEG-hy-c).* The unmodified and PEGylated MS NPs having a 42 nm diameter were prepared and purified as described in our previously reported method.[23]

Hydrothermally Treated Highly Organosilane-Modified MS NPs (MS42@PEG/TMS-hy-c, MS42@PEG/TFS-hy-c, and MS25@PEG/TMS-hy-c). First, 0.29 g of CTAB was added to 150 mL of 0.256 M NH_4OH solution, sealed, and continuously stirred for 1 h at 50 °C. Then, 2.5 mL of 0.88 M ethanolic TEOS solution was added to the solution under continuous stirring. After 1 h, 450 μL of PEG-silane was added to the as-synthesized colloidal solution. The mixture was stirred for 30 min, and then 68 μL of TMS (for preparation of MS42@PEG/TMS-hy-c) or 86 μL of TFS (for preparation of MS42@PEG/TFS-hy-c) was added. After another 30 min, stirring was stopped and the obtained colloidal solution was aged at 50 °C for 20 h. The as-synthesized modified MS NP solution was filtered with a 0.45 μm GHP filter and diluted to 50 mL with DI water. The filtered MS NP solution was then heated at 90 °C for 24 h in a sealed vessel for hydrothermal treatment. The surfactant removal steps followed the centrifugation method from previously reported work.[23] The filtered as-synthesized organomodified MS colloids were transferred to 50 mL of 6 g/L ethanolic ammonium nitrate by centrifugation (66226 *g*, 30 min) and heated to 60 °C for 1 h with stirring. The NPs were washed once using 95% EtOH and then transferred to 50 mL of acidic ethanol solution (1 mL of concentrated HCl/1 L of ethanol) via centrifugation and heated to 60 °C for 2 h under stirring. The extracted NPs were further washed with 95% ethanol and then 99.5% ethanol once. Finally, the surfactant-free MS42@PEG/TMS-hy-c or MS42@PEG/TFS-hy-c NPs were suspended in 99.5% ethanol and filtered using a 0.2 μm polytetrafluoroethylene (PTFE) filter. The final products were stored in one of two ways, either in 99.5% EtOH or as a dry powder at either room temperature (RT) or 4 °C until use. The dry powder of products was obtained by evaporation from an ethanolic NP solution under vacuum. For MS25@PEG/TMS-hy-c, the synthesis procedure was similar to MS42@PEG/TMS-hy-c; the differences were using 0.128 M NH_4OH solution instead of 0.256 M NH_4OH solution and changing PEG-silane and TMS amounts to 360 and 52 μL, respectively. In addition, the aging condition was changed to 12 h at 60 °C.

Redispersible Fluorescent (FITC-MS42@PEG/TMS-hy-c) and Magnetic MS NPs (Fe_3O_4@MS@PEG/TMS-hy-c). For synthesis of FITC-MS42@PEG/TMS-hy-c, 1.9 mg of FITC was first dissolved in 1 mL of 99.5% ethanol and 2 μL of APTES was then added to the FITC ethanolic solution to prepare the ethanolic FITC-APTES solution. The solution was

Scheme 1. Schematic Illustration of Synthesis Procedure for Highly Organomodified MS NPs

stirred under dark conditions for 18 h at room temperature. Next, 0.29 g of CTAB was added to 150 mL of 0.256 M NH_4OH solution at 50 °C. Then, 1 mL of ethanolic FITC-APTES solution and 2.5 mL of 0.88 M ethanolic TEOS solution were added simultaneously to the solution under continuous stirring. After 1 h, 450 μL of PEG-silane was added to the as-synthesized colloidal solution. The solution mixture was stirred for 30 min, and then 68 μL of TMS was added. After another 30 min, stirring was stopped and the obtained solution was aged at 50 °C for 20 h. The subsequent hydrothermal treatment and purification steps followed the procedure described previously. For synthesis of Fe_3O_4@MS@PEG/TMS-hy-c, the oleic acid-coated Fe_3O_4 was prepared based on a chemical coprecipitation method as described in our previously published work.[25] First, 5 mL of aqueous solution containing 0.29 g of CTAB and 0.2 g PVP was prepared. Then, 0.63 mL of 52 mg/mL hydrophobic Fe_3O_4 NPs (in chloroform) was added to the CTAB solution and ultrasonicated for 1 h to evaporate the chloroform and allow an aqueous suspension of the Fe_3O_4 NPs. The resulting Fe_3O_4 NP aqueous suspension was added to 150 mL of 0.256 M NH_4OH solution and heated to 50 °C for 1 h. The subsequent synthetic conditions were based on the procedure described in the synthesis of MS42@PEG/TMS-hy-c. Then, 3 mL of 0.88 M ethanolic TEOS solution was added. After 1 h, 540 μL of PEG-silane was added to the mixture solution, and 30 min later, 78 μL of TMS was added. After another 30-min stirring period, the obtained solution was aged at 50 °C for 20 h. The subsequent hydrothermal treatment and purification steps followed the procedure described previously.

Redispersity and Long-Term Particle Stability of MS NPs in Various Media. In this work, there were two ways to disperse purified NPs in DI water. For purified MS NPs suspended in 99.5% EtOH, the NPs were centrifuged, transferred to DI water, washed with DI water one time, and suspended at 2 mg/mL. For dry powder, 1 mL of DI water was added to 30 mg or 10 mg of organomodified or drug-loaded MS NP powder, respectively. The solution was sonicated for 5 min to homogenously redisperse the NPs. All the MS NP suspensions were diluted to 1 mg/mL in various media (PBS, DMEM+10%FBS, or SBF) by adding 2 mL of 2 mg/mL of MS NP stock solution in DI water to 2 mL of 2× PBS, DMEM+10%FBS, or SBF solutions. For long-term particle stability studies, the MS NP solutions were then aged for 15 days at 37 °C.

Quantification of Degraded Free Silicon from MS42-d and MS42@PEG/TMS-hy-c. Surfactant-free MS42-d and MS42@PEG/TMS-hy-c NPs were suspended in SBF at 1 mg/mL concentration. The MS NP solutions were aged in SBF at 37 °C. Then, 1 mL of the MS NP solution was taken from the solution at different time points. The aged MS NPs were separated by passing the aged solution through a Millipore Amicon Ultra centrifugal filter (MWCO 10 000) at 5250*g* for 5 min. The free degraded silicon concentration in the filtered solution was determined using a blue silicomolybdic assay (SMA) on a Perkin-Elmer Lambda 12 UV−vis spectrometer (Waltham, MA) at 810 nm. The details of the SMA have been described previously.[26] The silicon quantification was based on a calibration curve (0 ppm, 1 ppm, 5 ppm, 10 ppm, 20 ppm, 40 ppm, and 50 ppm Si in SBF) made before sample measurements. The silicon quantification was performed in three independent experiments.

Biocompatibility of MS42-d and MS42@PEG/TMS-hy-c. *MTT Viability Assay.* Human endothelial cells (CRL-2922) and human skin fibroblast cells (CRL-2522) were purchased from American Type Culture Center (ATCC). Typically, 6×10^4 cells were seeded in 96-well plates and cultured in DMEM (for endothelial cells) or MEM (for fibroblasts) supplemented with 10% FBS and 1% PS at 37 °C under 5% CO_2. After 24 h, the cells were incubated with 100 μL of different concentrations of MS42-d and MS42@PEG-hy-c NP suspensions in serum-free media for 24 h. After NP incubation, the cells were washed with 100 μL of serum-free DMEM two times and incubated with 100 μL of 0.5 mg/mL MTT media for 2 h at 37 °C under 5% CO_2. Finally, the medium was removed and water-insoluble purple formazan crystals were dissolved in 200 μL of DMSO. The plate was placed on a rocking shaker for at least 20 min, and then 100 μL of the DMSO solution in each well was transferred to a new 96-well plate. Optical density of the produced stain was monitored at 570 nm, with 655 nm as a reference, using a Bio-Rad microplate reader (Hercules, CA). The cell viability was calculated using eq 1. Cells without NP exposure were used as a control.

$$\text{viability from MTT assay } (\%) = \left(\frac{\text{sample abs}_{570\text{nm}-655\text{nm}}}{\text{control abs}_{570\text{nm}-655\text{nm}}}\right) \times 100 \quad (1)$$

Hemolysis Assay. Fresh EDTA-stabilized human whole blood samples were obtained from Memorial Blood Center (St. Paul, MN). The washed RBCs were prepared following our previously reported procedure.[27] To examine the hemolytic activity of MS42-d and MS42@PEG/TMS-hy-c NPs, 0.2 mL of diluted RBC suspension (around 4.5×10^8 cells/mL) was added to 0.8 mL of 250 μg/mL of MS NP suspension solutions in PBS. The final concentration of MS NPs was 200 μg/mL. DI water (+RBCs) and PBS (+RBCs) were used as the positive control and negative control, respectively. All the samples were placed on a rocking shaker in an incubator at 37 °C for 0.5, 1.5, or 3.0 h. After incubation, the samples were centrifuged at 10 016*g* for 3 min. The hemoglobin absorbance in the supernatant was measured at 540 nm, with 655 nm as a reference, using a Bio-Rad iMark microplate reader (Hercules, CA). Percentage of hemolysis was determined using eq 2.

$$\text{percent hemolysis } (\%) = \left(\frac{\text{sample abs}_{540\text{nm}-655\text{nm}} - \text{negative control abs}_{540\text{nm}-655\text{nm}}}{\text{positive control abs}_{540\text{nm}-655\text{nm}} - \text{negative control abs}_{540\text{nm}-655\text{nm}}}\right) \times 100 \quad (2)$$

Lactate Dehydrogenase (LDH) Assay. Membrane integrity of human platelets after MS42-d and MS42@PEG/TMS-hy-c exposure was examined using the LDH assay. The LDH activity was measured using a BioVision LDH cytotoxicity assay kit (Milpitas, CA). Washed human platelets were obtained based on a protocol previously developed by our group.[28] Typically, 0.1 mL of the washed platelets (around 2×10^8) was added to 0.4 mL of 250 μg/mL of MS NP suspensions in PBS. The final

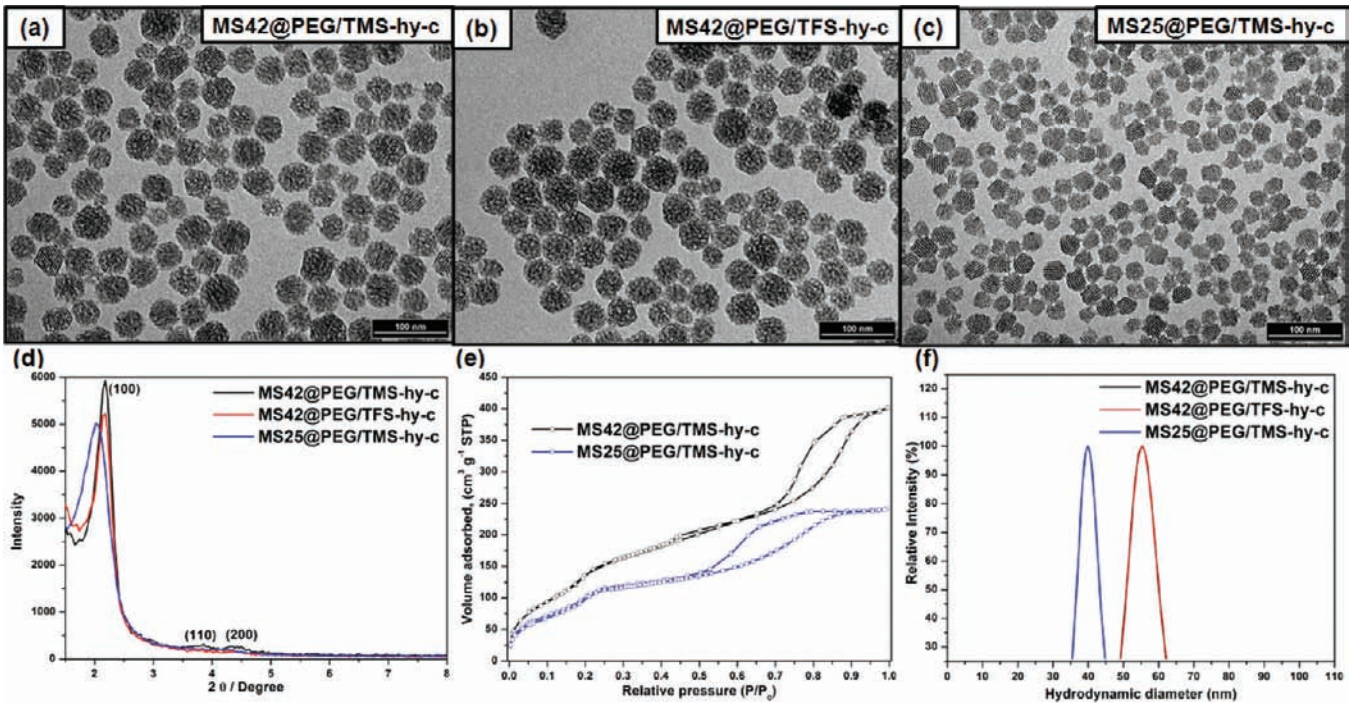

Figure 1. TEM images of extracted (a) MS42@PEG/TMS-hy-c, (b) MS42@PEG/TFS-hy-c, and (c) MS25@PEG/TMS-hy-c. (d) Powder XRD patterns of extracted MS42@PEG/TMS-hy-c, MS42@PEG/TFS-hy-c, and MS25@PEG/TMS-hy-c. (e) N_2 adsorption−desorption isotherms of extracted MS42@PEG/TMS-hy-c and MS25@PEG/TMS-hy-c. (f) Hydrodynamic size distributions of extracted MS42@PEG/TMS-hy-c, MS42@PEG/TFS-hy-c, and MS25@PEG/TMS-hy-c in SBF at RT (1 mg/mL).

NP concentration was 200 μg/mL. All the samples were placed on a rocking shaker in an incubator at 37 °C for 0.5, 1.5, or 3.0 h. After NP exposure, the solution was centrifuged at 1900*g* for 8 min. Then, 10 μL of supernatant was transferred to a 96-well plate and 100 μL of tetrazolium (WST-8) substrate mix was added. After 30 min, absorbance of the mixture solutions was measured at 450 nm with 655 nm as a reference, using a BioRad iMark microplate reader (Hercules, CA). The percent LDH release was calculated using eq 3. Cells without particle exposure and lysed with surfactant were used as the negative and positive control, respectively.

$$\text{percent LDH release}(\%) = \left(\frac{\text{sample abs}_{450\text{nm}-655\text{nm}} - \text{negative control abs}_{450\text{nm}-655\text{nm}}}{\text{positive control abs}_{450\text{nm}-655\text{nm}} - \text{negative control abs}_{450\text{nm}-655\text{nm}}}\right) \times 100 \quad (3)$$

Drug Loading and Delivery of MS42@PEG/TMS-hy-c. Two types of doxorubicin, water-soluble doxorubicin hydrochloride (DoxHCl), and poorly water-soluble doxorubicin (Dox) were loaded into M42@PEG/TMS-hy-c in this study. The poorly water-soluble Dox was prepared by adding equal volume of 0.5 mg/mL of DoxHCl to 0.001 M NaOH. After 10 h, the solution was centrifuged at 10 016*g* for 5 min. The obtained precipitated Dox was dried under vacuum. For drug loading conditions, about 10 mg of MS42@PEG/TMS-hy-c was added to 1 mL of 0.5 mg/mL of DoxHCl (in DI water) or 2 mL of 0.25 mg/mL of Dox (in DMSO/H_2O = 1:1 solution) solution and stirred for 24 h at RT. The drug-loaded NPs were collected by centrifugation (66 226*g*, 30 min) and washed with DI water one time. The obtained drug-loaded MS NPs were dried under vacuum. To determine the loaded amount of Dox in MS NPs, the drug-loaded NP powder (1.0−2.0 mg) was resuspended and ultrasonicated in 1 mL of DMSO and then allowed to stand overnight. Drug delivery from 1 mg/mL of DoxHCl-MS42@PEG/TMS-hy-c and Dox-MS42@PEG/TMS-hy-c was assessed in SBF at 37 °C using UV−vis absorbance of Dox at 480 nm. Dried drug-loaded MS NPs were redispersed in SBF, and the high salt concentration induced drug delivery. At each measurement time, a 1 mL of aliquot of the solution was collected and centrifuged. The obtained NPs were redispersed in SBF and added back to stock solutions of DoxHCl-MS42@PEG/TMS-hy-c and Dox-MS42@PEG/TMS-hy-c. The optical density of the supernatant was measured at 480 nm (655 nm as reference) using the microplate reader. The released free Dox was determined compared to a calibration curve.

In Vitro Therapeutic Efficacy of DoxHCl-MS42@PEG/TMS-hy-c and Dox-MS42@PEG/TMS-hy-c. HeLa cancer cells (6×10^3) were seeded in 96-well plates and cultured in DMEM supplemented with 10% FBS and 1% PS at 37 °C under 5% CO_2 for 24 h. The cells were incubated with 100 μL of the indicated concentrations of free DoxHCl, DoxHCl-MS42@PEG/TMS-hy-c, or Dox-MS42@PEG/TMS-hy-c. After different incubation periods (24, 48, or 72 h), the medium was removed and the cells were washed twice with serum-free DMEM. The procedure for measuring HeLa cell viability was the same as that described in the MTT viability assay.

Materials Characterization. *Transmission Electron Microscopy (TEM).* TEM micrographs were taken on a JEOL 1200 EXII (Tokyo, Japan) with a 100 kV voltage. TEM samples were prepared by dipping a Formvar-coated copper grid (Ted Pella, Redding, CA) into an ethanolic MS NP solution, and the grid was dried under air.

Powder X-ray Diffraction (XRD). XRD patterns were measured on a Siemens Bruker-AXS D-5005 X-ray diffractometer (Karlsruhe, Germany) using filtered Cu Kα radiation (λ = 1.5406 Å) at 45 kV and 20 mA. Data were recorded by step scan with a step size of 0.040° and a dwell time of 1.0 s.

N_2-Sorption Measurements. The N_2 adsorption−desorption isotherms were measured on a Quantachrom Autosorb-1 (Boynton Beach, FL) at 77K. The surface area and pore size of samples were determined by

Table 1. Physicochemical Characteristics of Highly Organomodified MS NPs[a]

sample	hydrodynamic size from as-synthesized particle (nm)	hydrodynamic size from powdered particle in water (nm)	hydrodynamic size from powdered particle in SBF (nm)	ζ-potential in water (mV)
MS42@PEG/TMS-hy-c	59.0 ± 1.6	59.4 ± 2.3	60.5 ± 0.80	−14.5 ± 1.1
MS42@PEG/TFS-hy-c	61.4 ± 0.81	58.3 ± 1.2	60.4 ± 3.3	−16.4 ± 1.4

[a] The NP concentration is 1 mg/mL. The measurements were taken at RT; values presented are mean ± SD from triplicate measurements.

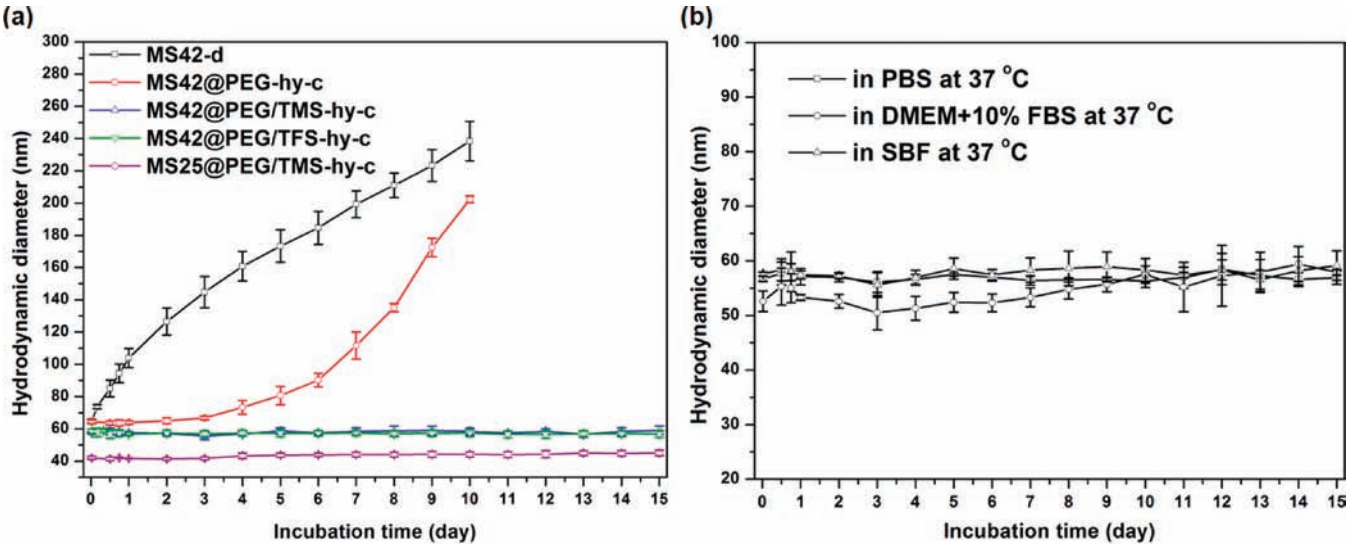

Figure 2. (a) Long-term colloidal stability of various MS NPs in SBF at 37 °C. (b) Long-term colloidal stability of MS42@PEG/TMS-hy-c NPs in various media: PBS, DMEM+10%FBS, and SBF at 37 °C.

the Brunauer−Emmett−Teller (BET) and Barret−Joner−Halenda (BJH) methods, respectively.

Dynamic Light Scattering (DLS). The hydrodynamic diameter measurements were carried out at either RT or 37 °C using DLS with a Brookhaven 90Plus particle analyzer (Holtsville, NY) equipped with a 35 mW red diode laser (660 nm). All the particles were suspended in various media at a NP concentration of 1 mg/mL and filtered through a 0.2 μm GHP filter to remove any possible dust. Three 1 min runs were performed on each measurement. The average DLS diameter was calculated from three independent samples. The DLS size distribution was plotted using a log-normal analysis method.

ζ-Potential Measurements. All MS NP solutions were prepared in DI water and SBF at a concentration of 1 mg/mL. ζ-potential was measured using a Brookhaven ZetaPALS Zeta-Potential Analyzer (Holtsville, NY). Five runs and ten cycles were set for each measurement. Each sample was measured three times.

^{29}Si Solid State NMR. Solid state ^{29}Si NMR spectra were recorded using a Varian VNMRS spectrometer operating at ^{1}H Larmor frequency of 700 MHz. Samples were spun at the magnetic angle (10 kHz) in a BioMAS Varian triple resonance probe. A single 90° pulse was applied to the ^{29}Si channel with ^{1}H decoupling during data acquisition. A recycle delay of 30 s was used between scans. The area of the Q^4, Q^3, and Q^2 peaks was calculated by Gaussian function fitting in OriginPro 8.5 software (Northampton, MA). Optical microscopy: Following 48-h exposure to DoxHCl-MS42@PEG/TMS-hy-c, the treated HeLa cells were washed with serum-free DMEM two times and observed under a Nikon Eclipse TE 2000-U inverted microscope (Melville, NY). The images were recorded using a Photometrics QuantEM 512SC camera (Tucson, AZ) with Meta-Morph imaging software (Molecular Devices, Downingtown, PA).

RESULTS AND DISCUSSION

MS NP Synthesis and Characterization. The synthesis procedure for hydrothermally treated, highly organosilane modified MS NPs followed in this work is shown in Scheme 1. To increase the dispersity and stability of the MS NPs, the as-synthesized bare MS NPs were simultaneously functionalized with two types of organosilane, a hydrophilic silane (polyethyleneglycol-silane, PEG-silane), and a hydrophobic silane (trimethylchlorosilane, TMS, or 3,3,3-trifluoropropyldimethylchlorosilane, TFS) before the surfactant removal step because irreversible aggregation often occurs during the surfactant removal process. In addition, hydrothermal treatment is a key step to increase the amounts of organosilane modified on the interior or exterior surface of MS NPs as demonstrated by our recently published work.[23] Herein, small MS NPs having 42 nm-diameter were modified with PEG/TMS or PEG/TFS using hydrothermal treatment and were purified by centrifugation (MS42@PEG/TMS-hy-c and MS42@PEG/TFS-hy-c, respectively). In addition, smaller MS NPs (25 nm-diameter) modified with PEG and TMS (denoted as MS25@PEG/TMS-hy-c) were also synthesized using this hydrothermal comodified method. Transmission electron microscopy (TEM) images of MS42@PEG/TMS-hy-c, MS42@PEG/TFS-hy-c, and MS25@PEG/TMS-hy-c are shown in Figure 1a−c. The TEM images show that both types of NPs have a hexagonal pore structure, regardless of different hydrophobic silane modification or size. However, the pore structure inside these NPs is somewhat disordered due to organosilane incorporation into the silica framework during the hydrothermal silica restructuring treatment. The detailed hexagonally ordered

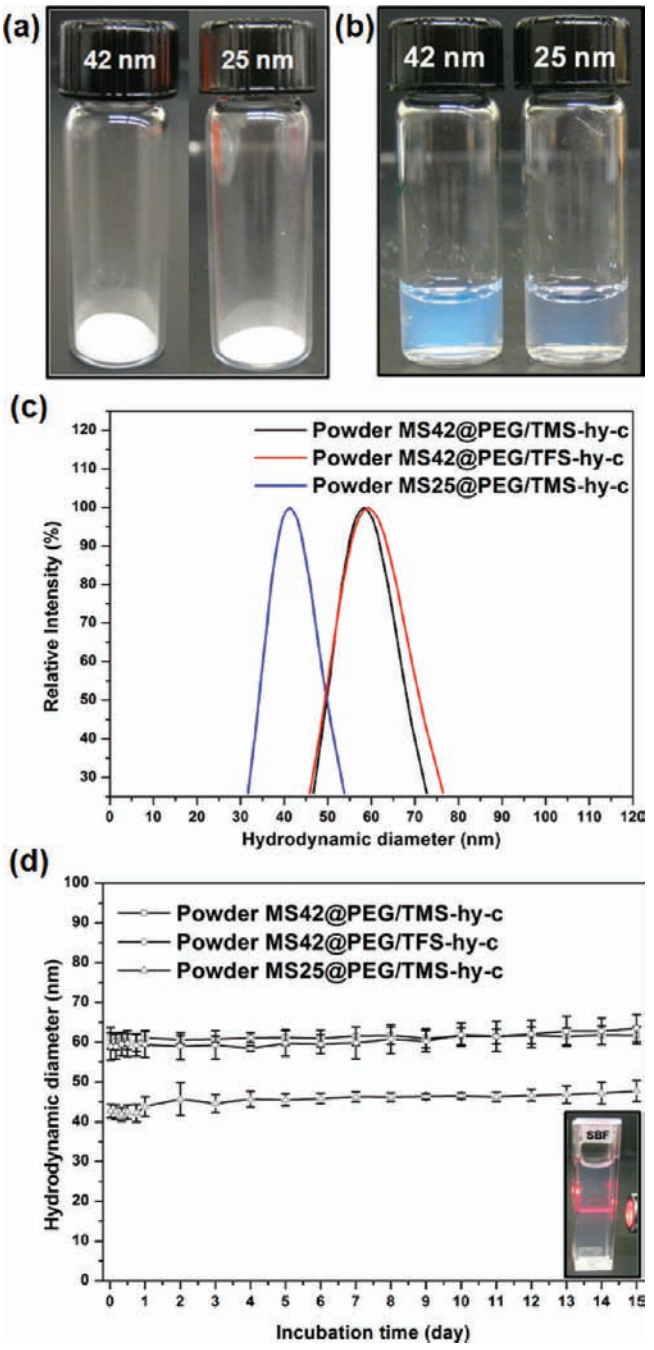

Figure 3. Digital pictures of (a) dry powder and (b) redispersed colloidal solution (30 mg/mL) of MS42@PEG/TMS-hy-c and MS25@PEG/TMS-hy-c. (c) Hydrodynamic diameter distributions of colloidal solutions prepared from MS42@PEG/TMS-hy-c, MS42@PEG/TFS-hy-c, and MS25@PEG/TMS-hy-c powder measured by DLS at RT in SBF. (d) Long-term stability of redispersed MS42@PEG/TMS-hy-c, MS42@PEG/TFS-hy-c, and MS25@PEG/TMS-hy-c NPs in SBF at 37 °C. Data represent mean ± SD from three independent experiments. Inset: a digital picture of MS42@PEG/TMS-hy-c colloidal solution prepared from MS42@PEG/TMS-hy-c powder after 15-day aging in SBF at 37 °C.

cylindrical pore structures of MS42@PEG/TMS-hy-c, MS42@PEG/TFS-hy-c, and MS25@PEG/TMS-hy-c NPs are shown in the Supporting Information (Figure S1). Only one strong peak (100) was detected in the low angle X-ray diffraction (XRD) patterns of MS42@PEG/TMS-hy-c, MS42@PEG/TFS-hy-c, and MS25@PEG/TMS-hy-c (Figure 1d), further confirming the two-dimensional hexagonal pore ordering inside particles observed in TEM images. Compared to MS42@PEG/TMS-hy-c, the (100) peak of MS25@PEG/TMS-hy-c is broader because of the short-range ordering of pore structure inside the particle. The N_2 adsorption−desorption measurements of MS42@PEG/TMS-hy-c and MS25@PEG/TMS-hy-c show that both particles exhibit a typical type IV isotherm (Figure 1e). The surface areas of MS42@PEG/TMS-hy-c and MS25@PEG/TMS-hy-c were 629 m^2/g and 498 m^2/g, respectively. Compared to the high surface area (1163 m^2/g) of unmodified MS NPs (MS42-d) reported in our recent published work,[23] a large surface area decrease occurred for these organomodified MS NPs. Also, there was a large decrease in pore diameter from 2.4 nm for MS42-d to 1.6 nm for MS42@PEG/TMS-hy-c. These results support that large amounts of short-length PEG and TMS were indeed incorporated and modified either outside or inside the pores during the hydrothermal treatment, causing the decrease in pore size and surface area.

Dispersity and Stability of Hydrothermally Treated Dual-Organosilane Modified MS NPs. To examine the dispersity of these organomodified MS NPs, they were directly transferred to a highly salted medium, SBF by centrifugation, and their hydrodynamic size was measured using DLS. As shown in Figure 1f, the hydrodynamic size distributions of MS42@PEG/TMS-hy-c and MS42@PEG/TFS-hy-c were almost identical, and each had a hydrodynamic size of approximately 60 nm in SBF. Compared to the hydrodynamic size of as-synthesized MS42@PEG/TMS-hy-c and MS42@PEG/TFS-hy-c listed in Table 1, the hydrodynamic size of these modified NPs was still around 60 nm in SBF after nine repeated high-speed centrifugation and ultrasonication steps during the surfactant removal and redispersion process. In addition, the smaller MS25@PEG/TMS-hy-c NPs were also well-dispersed in SBF and had a hydrodynamic size of 40 nm, which was almost the same as the as-synthesized MS25@PEG/TMS-hy-c. All the polydispersity values (determined by DLS) of MS42@PEG/TMS-hy (0.005), MS42@PEG/TFS-hy-c (0.004), and MS25@PEG-hy-c (0.014) NPs in SBF are close to zero, indicating that the samples are monodisperse, uniform, and well-dispersed in SBF. These results showed that modifying the MS NPs with hydrophilic and hydrophobic silane can greatly improve their dispersity. However, the single time measurement of the hydrodynamic size of NPs only shows short-term stability (minutes). Long-term (days) particle stability of three types of MS NPs: bare MS NPs (MS42-d), highly PEGylated MS NPs (MS42@PEG-hy-c), and highly PEG/TMS dual-modified MS NPs (MS42@PEG/TMS-hy-c) was measured in biological media, including PBS, cell culture media (Dulbecco's Modified Eagle's Medium+10% fetal bovine serum, DMEM+10%FBS), and SBF at 37 °C. As shown in Figure 2a, the hydrodynamic size of MS42-d and MS42@PEG-hy-c in SBF increases over time. This result shows that these particles form irreversible aggregates in a biologically relevant environment. Interestingly, MS42@PEG-hy-c increased in size at a much slower rate, but MS42@PEG/TMS-hy-c and MS42@PEG/TFS-hy-c did not increase in size at all over a 15 day incubation period (Figure 2a), showing that the additional hydrophobic silane modification/incorporation on/into MS NPs improved the stability of hydrothermally treated PEGylated MS NPs. For the smaller MS25@PEG/TMS-hy-c NPs, no size change was observed even after 15-day aging in SBF at 37 °C. In addition, no significant size change of MS42@PEG/TMS-hy-c

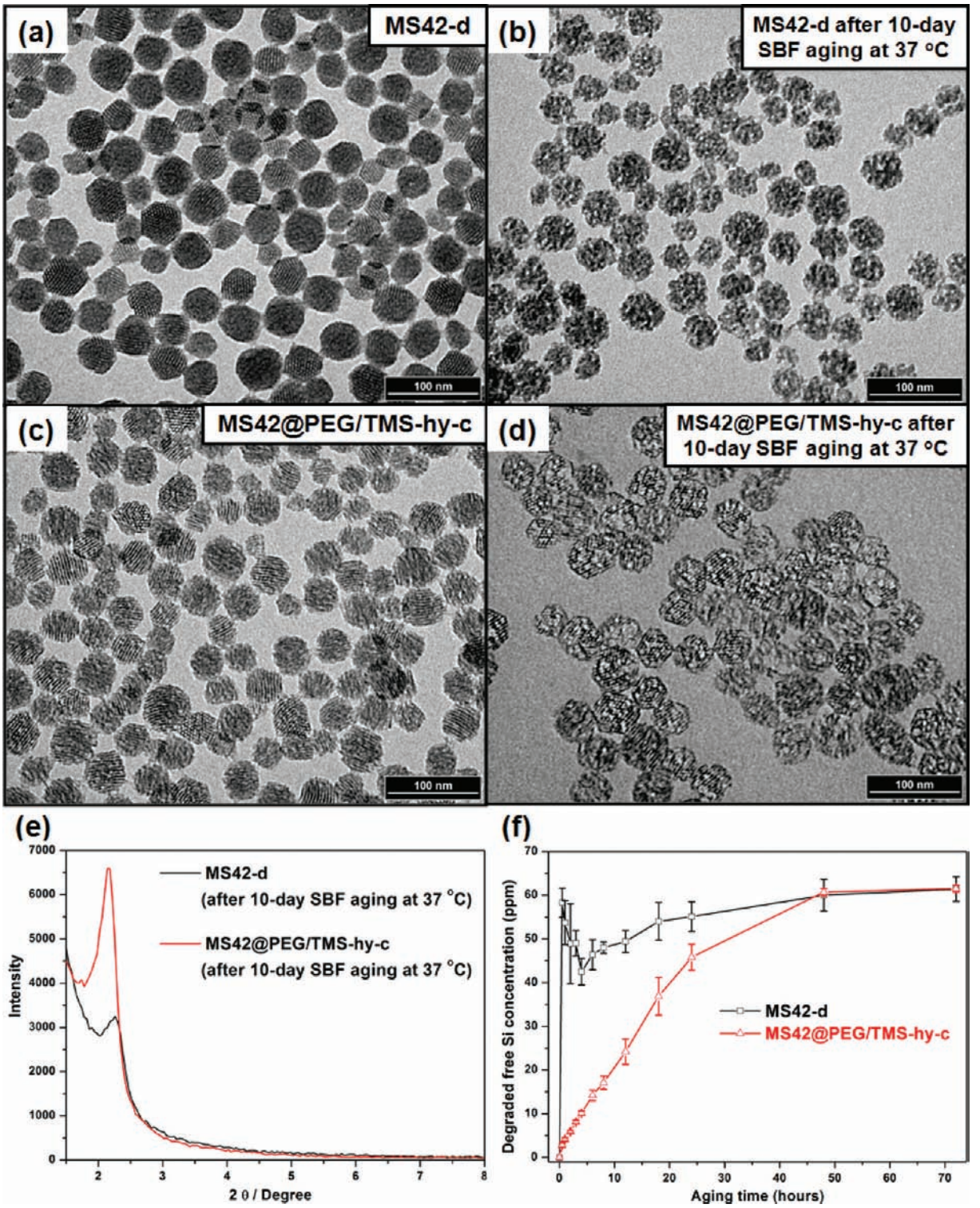

Figure 4. TEM images of extracted MS42-d and MS42@PEG/TMS-hy-c before (a, c) and after (b, d) 10-day SBF aging at 37 °C. (e) XRD patterns of extracted MS42-d and MS42@PEG/TMS-hy-c after 10-day SBF aging at 37 °C. (f) Degraded free silicon amount from 1 mg/mL of MS42-d and MS42@PEG/TMS-hy-c colloidal solutions in SBF at 37 °C.

in other biological media after 15-day aging at 37 °C was observed (Figure 2b). All these results confirm that dual-silane surface modification via hydrothermal treatment significantly improves the MS NP stability in various biologically relevant media, even with a particle size as small as 25 nm.

Another common problem in various nanotherapeutic candidates is irreversible aggregation once the NPs are dried. The redispersity of hydrothermally treated dual-organosilane-modified NP powder was evaluated by drying the NPs from ethanolic suspensions using rotary evaporation (Figure 3a) and simply

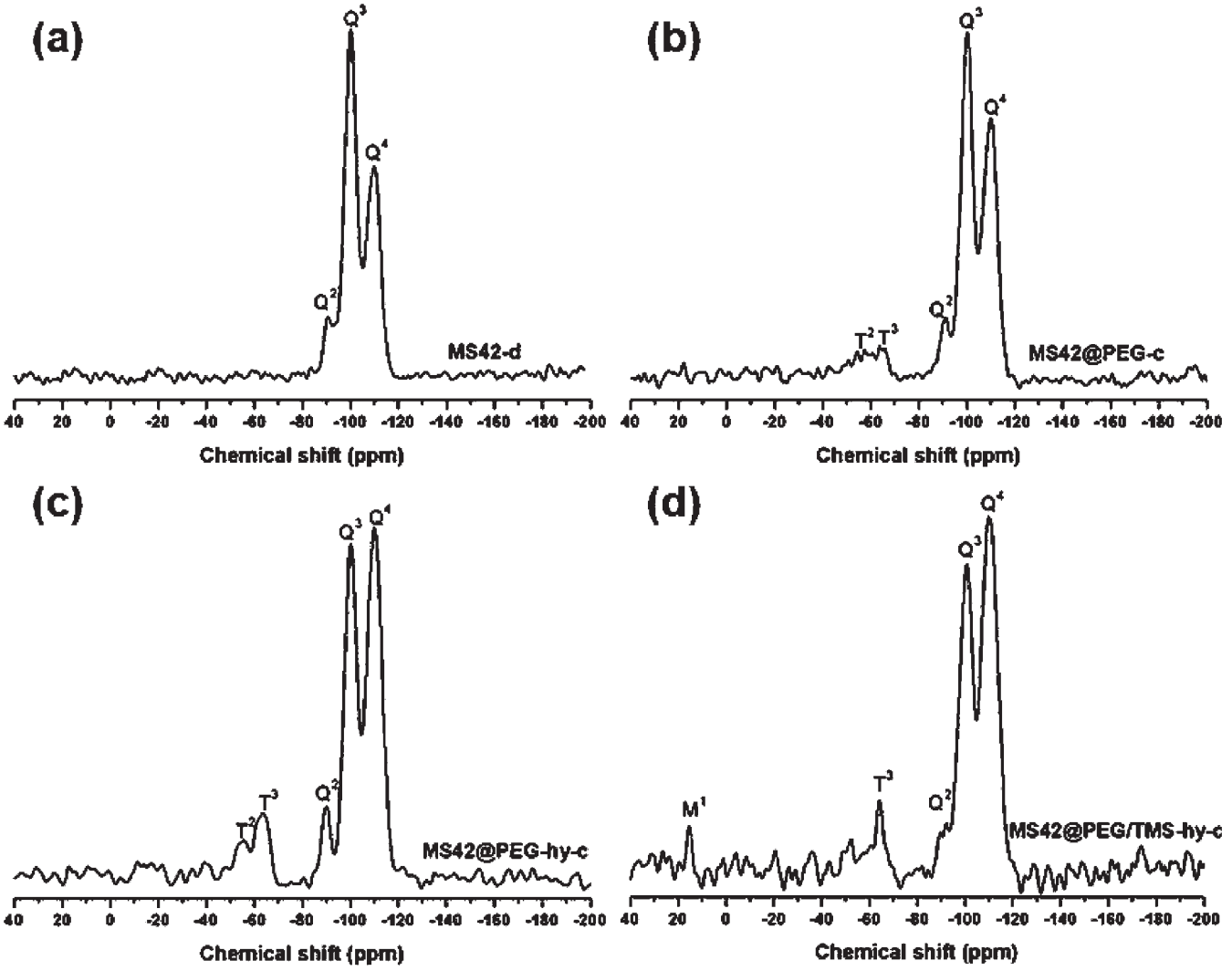

Figure 5. ^{29}Si solid-state MAS NMR spectra of (a) MS42-d, (b) MS42@PEG-c, (c) MS42@PEG-hy-c, and (d) MS42@PEG/TMS-hy-c.

redispersing the NP powder in DI water by ultrasonication for 5 min. One can clearly see well-suspended, optically transparent colloidal solutions (Figure 3b) prepared from either MS42@PEG/TMS-hy-c or MS25@PEG/TMS-hy-c powders. The hydrodynamic size distributions of MS42@PEG/TMS-hy-c, MS42@PEG/TFS-hy-c, and MS25@PEG/TMS-hy-c NP solutions prepared from the powder samples are shown in Figure 3c. The hydrodynamic size of dried MS42@PEG/TMS-hy-c and MS42@PEG/TFS-hy-c was ~60 nm in DI water and almost identical to as-synthesized MS42@PEG/TMS-hy-c and MS42@PEG/TFS-hy-c (Table 1). Even for MS25@PEG/TMS-hy-c with smaller diameter, the dried NPs can be reversibly dispersed into aqueous solution, and their hydrodynamic size was maintained at ~40 nm (Figure 3c). In addition, no substantial hydrodynamic size change (Figure 3d) or visible particle precipitate (inset photograph of Figure 3d) was observed for any of the NP solutions prepared from MS42@PEG/TMS-hy-c, MS42@PEG/TFS-hy-c, and MS25@PEG/TMS-hy-c powders after 15-day aging in SBF at 37 °C. This result is a vast improvement over previous published work on improving MS NP dispersity.[18−23] To the best of our knowledge, this is the first work synthesizing highly stable and redispersible MS NPs.

Degradation of Hydrothermally Treated Dual-Organosilane Modified MS NPs. A variety of methods were used to study the degradation of MS NPs in biological media. TEM images taken before and after 10-day SBF aging at 37 °C showed that MS42-d experienced a decrease in diameter (Figure 4a,b and see the Supporting Information, S2a,b) and had almost completely lost its porous structure following aging while MS42@PEG/TMS-hy-c showed some degradation but still retained its size and porous structure (Figure 4c,d and see the Supporting Information, S2c,d). XRD patterns of the MS42-d and MS42@PEG/TMS-hy-c after 10-day SBF aging further confirmed that pore collapse was much more pronounced for MS42-d in SBF (Figure 4e). Colorimetric silicon assays showed that MS42-d experienced fast bulk silica degradation, followed by a decrease in silicon amount because of the formation and deposition of magnesium/calcium silicon layers on/in MS NPs and a subsequent slow dissolution process. This result is similar to a published work reported by Shi and co-workers.[29] In contrast, MS42@PEG/TMS-hy-c had a much slower dissolution behavior and degradation rate (Figure 4f) than that of MS42-d. In addition, ^{29}Si solid-state MAS NMR was used to investigate the degree of silica condensation and connectivity of the organic groups to the

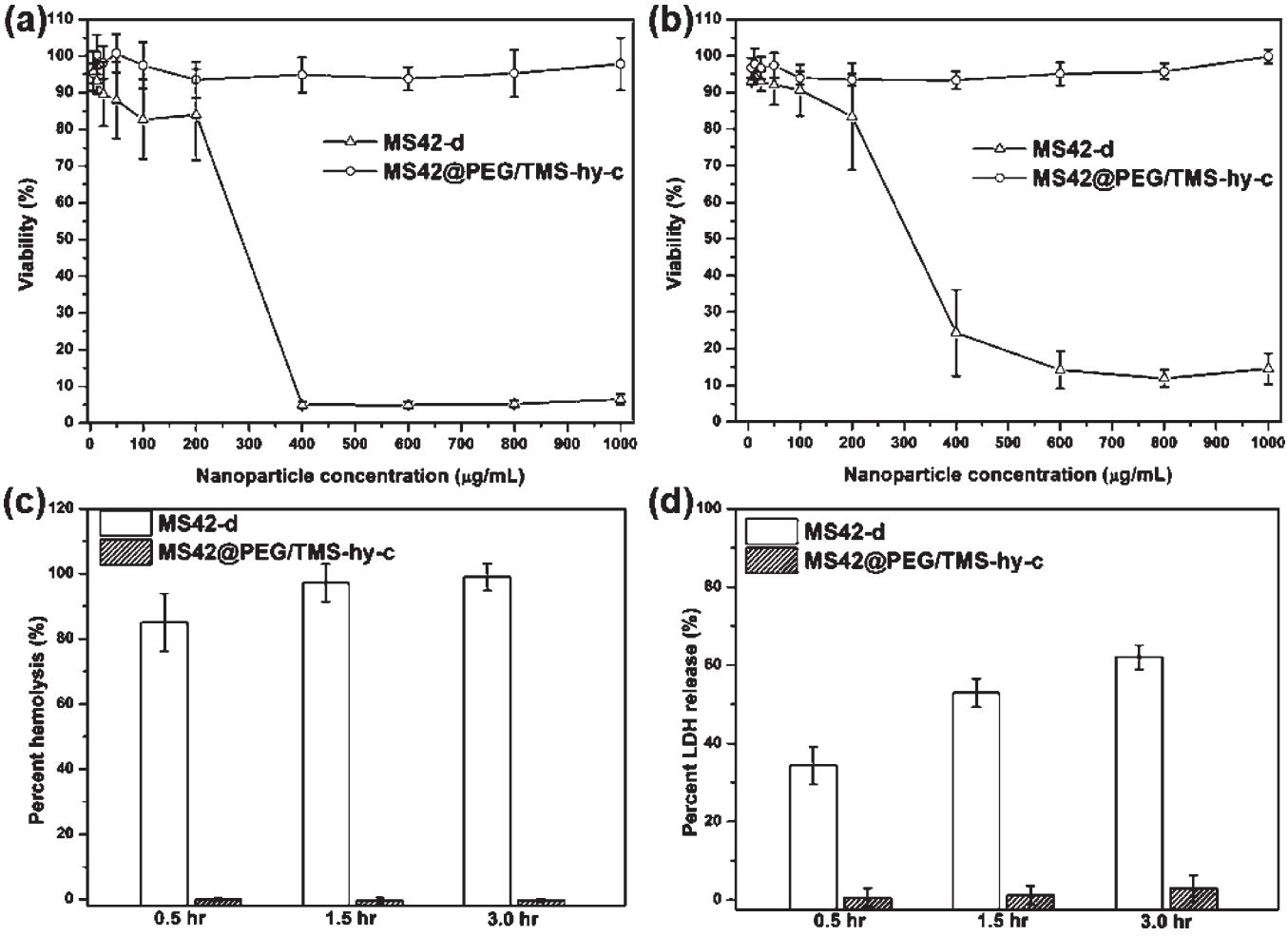

Figure 6. Viability of (a) human endothelial cells and (b) human skin fibroblasts after 24 h exposure at different concentrations of MS42-d and MS42@PEG/TMS-hy-c. (c) Percentage of hemolysis of RBCs and (d) percent LDH leakage from human platelets after exposure to 200 μg/mL of MS42-d and MS42 MS42@PEG/TMS-hy-c for 0.5, 1.5, or 3.0 h at 37 °C.

silica framework in four types of MS NPs: MS42-d, MS42@PEG-c, MS42@PEG-hy-c, and MS42@PEG/TMS-hy-c (Figure 5). Spectra for all four types of MS NPs showed three peaks at −110 ppm (Q^4, $Si(OSi)_4$), −100 ppm (Q^3, $Si(OSi)_3(OH)$, and −90 ppm (Q^2, $Si(OSi)_2(OH)_2$). Q^4, Q^3, and Q^2 represent fully condensed silica, silica with one terminal hydroxyl group, and silica with germinal hydroxyls, respectively. For MS42@PEG-c and MS42@PEG-hy-c, two additional peaks were observed at −68 ppm (T^3, $R\text{-}Si(OSi)_3$) and −58 ppm (T^2, $R\text{-}Si(OSi)_2(OH)$), corresponding to the PEG-silane modification and incorporation into the MS NPs (Figure 5b and 5c). For MS42@PEG/TMS-hy-c, one more additional peak was detected at 15 ppm (M^1, R3-Si(OSi), indicating the trimethyl group functionalization on/in the MS NPs. The relative ratio of partially and fully condensed silicon sites $[(Q^3+Q^2)/Q^4]$ calculated by integrating the peak areas yields an estimate of the degree of condensation in the silica framework. The $(Q^3+Q^2)/Q^4$ ratios for MS42-d, MS42@PEG-c, MS42@PEG-hy-c, and MS42@PEG/TMS-hy-c are 1.6, 1.3, 0.90, and 0.77, respectively. This result shows that organosilane modification and hydrothermal treatment greatly increased the amount of fully condensed silica. In addition, compared to the highly negative charge on the MS42-d (−34.5 mV), a large decrease in surface charge on MS42@PEG/TMS-hy-c (−14.5 mV) and MS42@PEG/TFS-hy-c (−16.4 mV), as measured using ζ-potential analysis, further confirmed that most of the surface silanol groups were eliminated by PEG and TMS functionalization through the hydrothermal process. In summary, the high stability of these organomodified MS NPs was due to more fully condensed silica and more organosilane anchored during hydrothermal treatment. These changes resulted in higher resistance to silica dissolution (biodegradation) due to increased hydrophobicity[30] and prevention of pore collapse[23] and irreversible aggregation from silica deposition[29,31] on the particles. Additionally, the high redispersity is likely attributable to large amounts of organosilane modification, completely eliminating either the outer surface or interior silanol groups.

In Vitro Biocompatibility of Hydrothermally Treated Organomodified MS NPs. The biocompatibility of MS42-d and MS42@PEG/TMS-hy-c was first assessed by incubating the nanoparticles with human endothelial and skin fibroblast cells. Compared to a significant decrease in viability caused by MS42-d as the NP concentration exceeded 200 μg/mL, the MS42@PEG/TMS-hy-c NPs did not influence either the human endothelial or skin fibroblast cell viability even after 24-h exposure at 1000 μg/mL (Figure 6a and 6b). In addition, no significant reactive oxygen

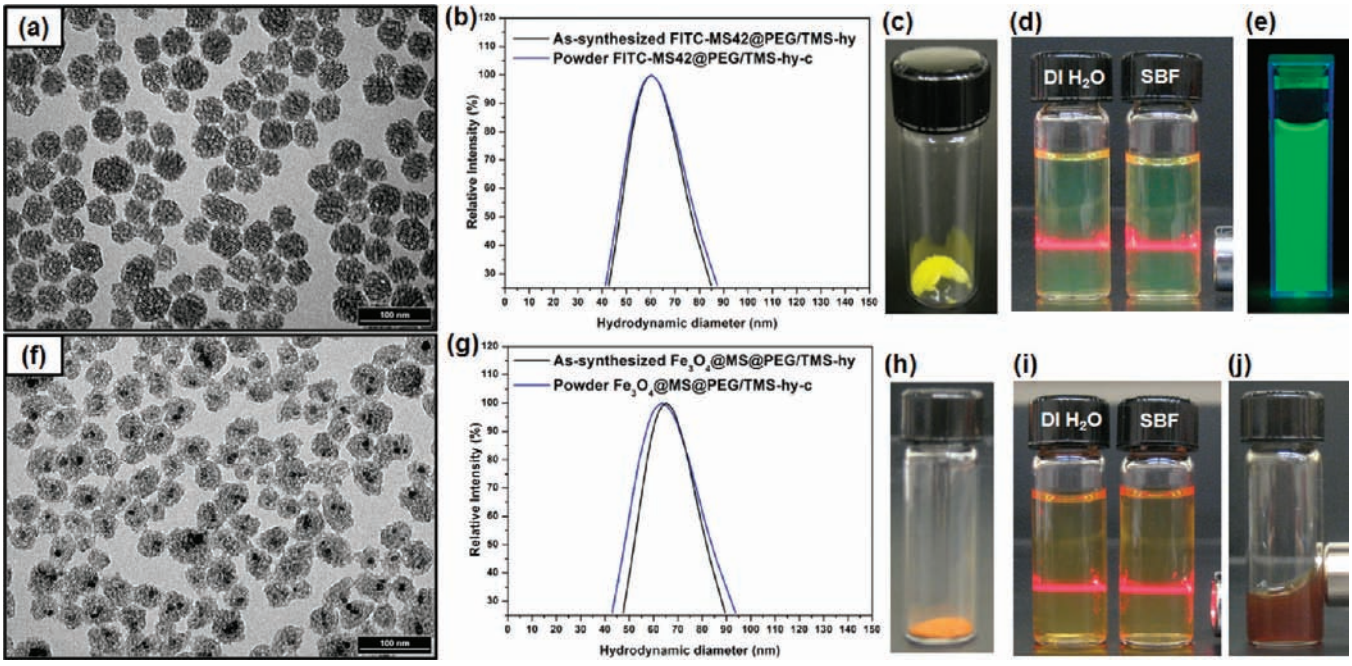

Figure 7. (a) The TEM image, (b) hydrodynamic diameter distributions, (c) powder and (d) colloidal solutions (1 mg/mL) of surfactant-free FITC-MS42@PEG/TMS-hy-c NPs. (e) A photograph of 1 mg/mL of redispersed FITC-MS42@PEG/TMS-hy-c in SBF under UV illumination. (f) The TEM image, (g) hydrodynamic diameter distributions, (h) powder, and (i) colloidal solutions (1 mg/mL) of surfactant-free Fe_3O_4@MS@PEG/TMS-hy-c. (j) A photograph of 30 mg/mL of redispersed Fe_3O_4@MS@PEG/TMS-hy-c in DI water during exposure to a magnet.

species were generated by MS42@PEG/TMS-hy-c in human endothelial cells after 24-h exposure (see the Supporting Information, Figure S3), showing that the PEG and TMS modification did not produce species that were cytotoxic to mammalian cells. Since the MS42@PEG/TMS-hy-c is designed to be intravenously injected, its compatibility to red blood cells (RBCs) and platelets was also examined by hemolysis and a lactate dehydrogenase (LDH) assay. Following a similar trend, 200 μg/mL of MS42-d NPs caused significant membrane damage in RBCs (>90% cell lysis) and platelets (>60% cell lysis) after 3-h incubation, but almost zero percent hemoglobin and LDH release occurred after 200 μg/mL of MS42@PEG/TMS-hy-c NP exposure (Figure 6c and 6d). These results show that MS42@PEG/TMS-hy-c NPs are much more biocompatible than unmodified MS NPs and that the additional TMS modification does not cause any damage or produce toxic species. In addition, our very recent work studying the cytotoxicity of MS42-d and MS42@PEG/TMS-hy-c NPs under flow conditions with different shear stress further confirmed high biocompatibility of MS42@PEG/TMS-hy-c NPs.[32]

Redispersible Fluorescent, Magnetic, and Anticancer Drug-Loaded MS NPs. To further demonstrate the versatility of this hydrothermal-assisted dual-organosilane modification method, fluorescent and magnetic functionality were incorporated into these ultrastable, redispersible, small, and highly organomodified MS NPs. First, a green fluorescent MS NP, called FITC-MS42@PEG/TMS-hy-c, was prepared by incorporating FITC into the MS42@PEG/TMS-hy-c with a commonly used co-condensation method.[33] The TEM image of FITC-MS42@PEG/TMS-hy-c showed no size or morphology change after FITC incorporation compared to MS42@PEG/TMS-hy-c (Figure 7a). To study the redispersity of FITC-MS42@PEG/TMS-hy-c, the dried powder of FITC-MS42@PEG/TMS-hy-c was redispersed into DI water by ultrasonication, and its hydrodynamic size was measured using DLS (Figure 7b and 7c). The hydrodynamic size distribution of as-synthesized FITC-MS42@PEG/TMS-hy-c and powdered FITC-MS42@PEG/TMS-hy-c confirmed the excellent redispersity of FITC-MS42@PEG/TMS-hy-c. Yellowish and transparent NP solutions (in DI water or SBF) showing Tyndall light scattering behavior were prepared from powdered FITC-MS42@PEG/TMS-hy-c samples (Figure 7d). The fluorescence of FITC-MS42@PEG/TMS-hy-c under UV illumination was homogeneously distributed in SBF (Figure 7e).

Similarly, the magnetic MS NPs, denoted as Fe_3O_4@MS@PEG/TMS-hy-c, were synthesized using Fe_3O_4 NPs as cores upon which the MS shell was deposited. Figure 7f shows that Fe_3O_4 NPs were successfully coated with a MS shell and functionalized with PEG/TMS. The Fe_3O_4@MS@PEG/TMS-hy-c NPs can be simply synthesized by adding Fe_3O_4 NPs prior to the silica condensation step in the synthesis procedure of MS42@PEG/TMS-hy-c. Again, the comparison of hydrodynamic size distribution (Figure 7g) between as-synthesized Fe_3O_4@MS@PEG/TMS-hy-c NP solution and Fe_3O_4@MS@PEG/TMS-hy-c solution prepared from powder samples (Figure 7h) showed the great resdispersity of Fe_3O_4@MS@PEG/TMS-hy-c powder. The homogeneous (Figure 7i) and clear NP solutions in DI water and PBS were prepared from Fe_3O_4@MS@PEG/TMS-hy-c powder. In addition, magnetic response of the NP solution was observed by placing a strong neodymium magnet close to the vial (Figure 7j). It is worth mentioning that no NP separation from the solution over a long period of time (>2 h) further confirmed the truly redispersible nature of Fe_3O_4@MS@PEG/TMS-hy-c and extremely high colloidal stability of resuspended Fe_3O_4@MS@PEG/TMS-hy-c NPs.

To explore the capability of the ultrastable MS42@PEG/TMS-hy-c NPs as anticancer drug delivery carriers, two types of

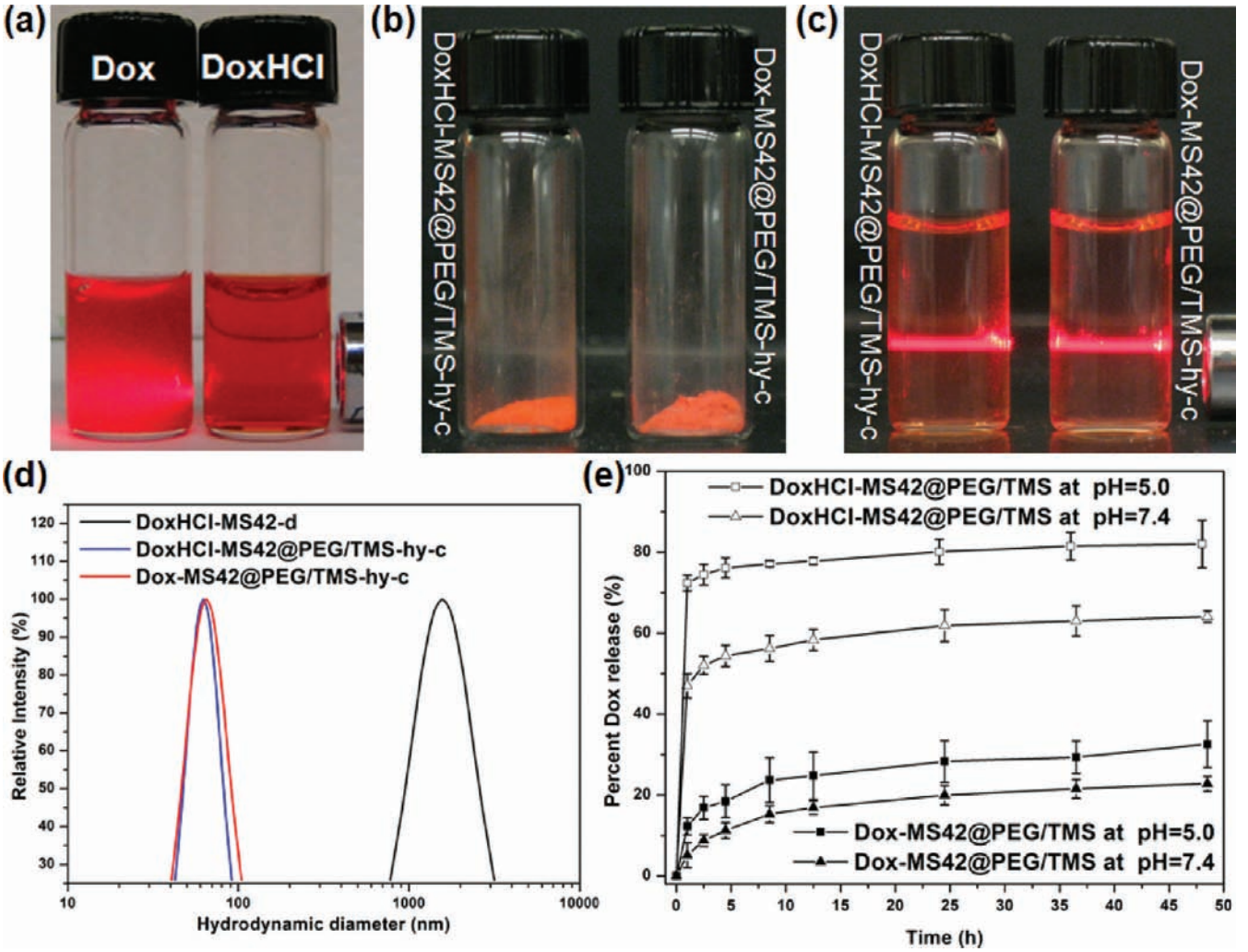

Figure 8. Photographs of (a) 1 mM Dox and DoxHCl solutions, (b) powder, and (c) colloidal solutions of DoxHCl-MS42@PEG/TMS-hy-c and Dox-MS42@PEG/TMS-hy-c. (d) Hydrodynamic size distributions of redispersed DoxHCl-MS42-d, DoxHCl-MS42@PEG/TMS-hy-c, and Dox-MS42@PEG/TMS-hy-c. (e) Drug release profile from DoxHCl-MS42@PEG/TMS-hy-c and Dox-MS42@PEG/TMS-hy-c at pH 7.4 and pH 5.0 ($n \geq 3$).

Table 2. IC_{50} of Free DoxHCl, DoxHCl-MS42@PEG/TMS-hy-c, and Dox-MS42@PEG/TMS-hy-c after 24, 48, or 72h Incubation with HeLa Cells

incubation time (hours)	free DoxHCl (μM Dox)	DoxHCl-MS42@PEG/TMS-hy-c (μM Dox)	Dox-MS42@PEG/TMS-hy-c (μM Dox)
24	0.78	0.75	8.1
48	0.072	0.047	0.73
72	0.053	0.042	0.51

doxorubicin, water-soluble doxorubicin hydrochloride (DoxHCl), and poorly water-soluble doxorubicin (Dox) were loaded to MS42@PEG/TMS-hy-c NPs, denoted as DoxHCl-MS42@PEG/TMS-hy-c and Dox-MS42@PEG/TMS-hy-c, respectively. As shown in Figure 8a, DoxHCl can be completely dissolved in water but Dox formed significant aggregates in water. The DoxHCl and Dox loading into MS42@PEG/TMS-hy-c NPs were easily confirmed by the red color from drug-loaded MS42@PEG/TMS-hy-c NPs after separation from the NP-incubated doxorubicin solutions by ultracentrifugation. The loading weight percentages (compared to overall weight of the particle) of DoxHCl and Dox in MS42@PEG/TMS-hy-c NPs were 3.0% and 2.8%, respectively. The DoxHCl-MS42@PEG/TMS-hy-c and Dox-MS42@PEG/TMS-hy-c were dried under vacuum (Figure 8b) and redispersed into DI water by ultrasonication. Both DoxHCl-MS42@PEG/TMS-hy-c and Dox-MS42@PEG/TMS-hy-c powders can be resuspended, forming transparent aqueous solutions without observable precipitate (Figure 8c). Although doxorubicin-loaded MS NPs have precedent in the literature,[20,34,35] none of the previous work has shown the hydrodynamic size or examined the particle dispersity after drug loading. Compared to a large hydrodynamic size (>2000 nm) of resuspended DoxHCl-loaded MS42-d (denoted as DoxHCl-MS42-d) NP solution, the hydrodynamic sizes of redispersed DoxHCl-MS42@PEG/TMS-hy-c and Dox-MS42@PEG/TMS-hy-c NP solutions were both retained around 60 nm (Figure 8d), further showing that MS42@PEG/TMS-hy-c NPs can be used as excellent drug carriers, especially to improve the dispersity/solubility of poorly soluble drugs or hydrophobic drugs in aqueous solutions. In addition, even though the MS42-d NPs have higher loading capacity (4.5%) for DoxHCl, the poor dispersity, stability, and large hydrodynamic size (Figure 8d) of unmodified

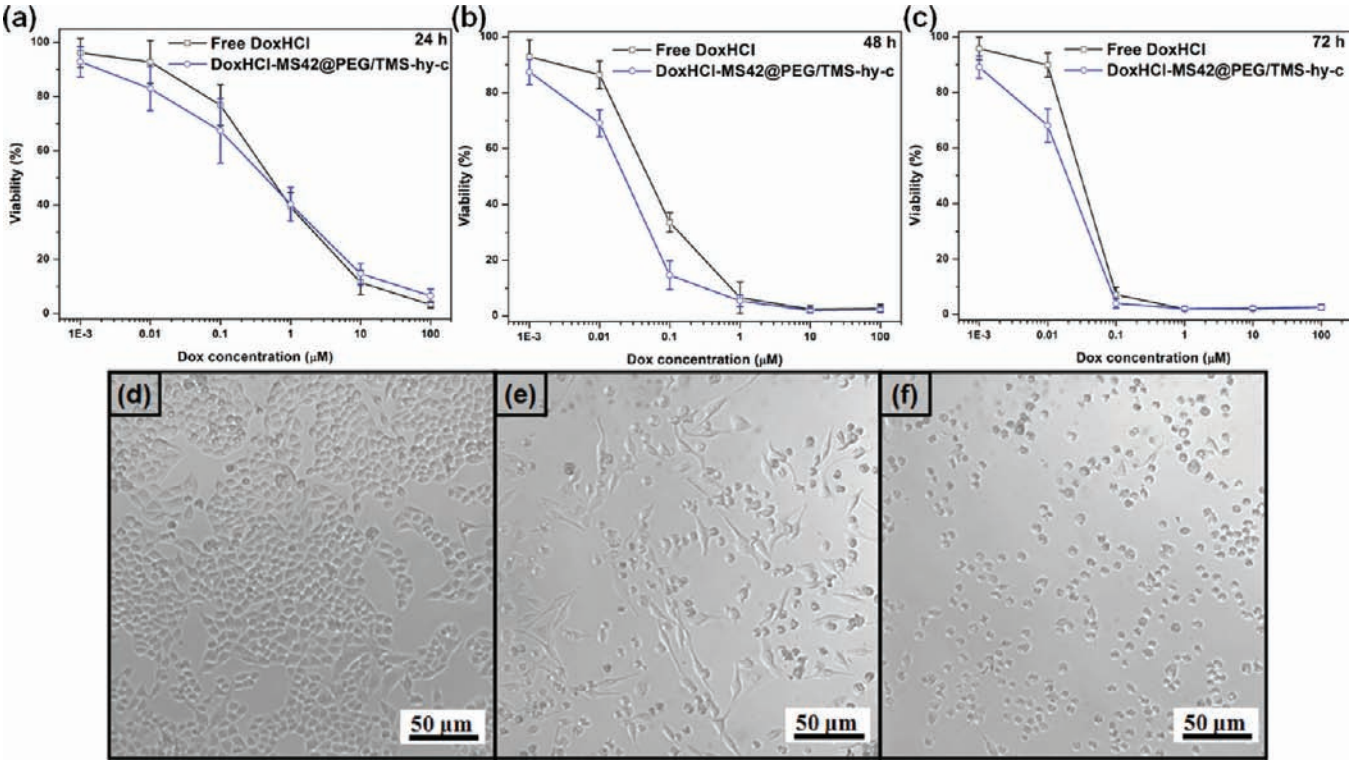

Figure 9. Cytotoxicity profile of DoxHCl-MS42@PEG/TMS-hy-c at equivalent free DoxHCl dose incubated with HeLa cells for (a) 24, (b) 48, or (c) 72 h. Data represent mean ± SD from at least three independent experiments done in triplicate. Optical micrographs of HeLa cells after 48 h incubation with (d) medium (control), (e) free HCl, and (f) DoxHCl-MS42@PEG/TMS-hy-c. The doxorubicin concentration was 0.1 μM.

DoxHCl-MS42-d NPs in aqueous solution greatly limit their potential use in vivo.

Drug Delivery and Cytotoxic Efficacy of Hydrothermally Treated Organomodified MS NPs. Cumulative drug release profiles for DoxHCl-MS42@PEG/TMS-hy-c and Dox-MS42@PEG/TMS-hy-c in SBF (pH = 7.4 and 5.0) at 37 °C are shown in Figure 8e. DoxHCl-MS42@PEG/TMS-hy-c exhibited very quick burst release (~50% of drug release within 1 h at pH = 7.4), followed by a sustained, relatively slow release (~60% of drug release within 48 h at pH = 7.4). The initial rapid release rate from DoxHCl-MS42@PEG/TMS-hy-c NPs is likely attributable to the high solubility of DoxHCl and the DoxHCl drugs held weakly or without interaction to the interior surface of MS42@PEG/TMS-hy-c. Compared to DoxHCl-MS42@PEG/TMS-hy-c, Dox-MS42@PEG/TMS-hy-c showed a much slower initial release rate and lower released amounts (less than 20% of drug release within 48 h at pH = 7.4) because of the low solubility of Dox and strong hydrophobic interactions between Dox and TMS. This is the first example showing that the release behavior of doxorubicin from MS NPs depends on the solubility of doxorubicin. Furthermore, both DoxHCl-MS42@PEG/TMS-hy-c and Dox-MS42@PEG/TMS-hy-c exhibited faster release rate and greater release amounts in mildly acidic condition (pH = 5.0) due to higher solubility of both DoxHCl and Dox at lower pH (more protonated NH_2 groups on DoxHCl and Dox). This acidic environment will be relevant if the drug delivery nanoparticles are ever taken up into intracellular acidic organelles.[15−17]

To examine whether the released doxorubicin was still able to kill cancer cells, the cytotoxic efficacy of DoxHCl-MS42@PEG/TMS-hy-c and Dox-MS42@PEG/TMS-hy-c on HeLa cells was investigated. The HeLa cells were incubated with either free DoxHCl, DoxHCl-MS42@PEG/TMS-hy-c, or Dox-MS42@PEG/TMS-hy-c at equivalent doxorubicin doses for 24, 48, or 72 h. The half maximal inhibitory concentration of doxorubicin (IC_{50}) was determined by MTT viability data. The comparison of cytotoxcity and IC_{50} of free DoxHCl and DoxHCl-MS42@PEG/TMS-hy-c on HeLa cells is shown in Figure 9a−c and Table 2. These data reveal that free DoxHCl and DoxHCl-MS42@PEG/TMS-hy-c have similar cytotoxicity to HeLa cells after 24-h incubation, and then MS42@PEG/TMS-hy-c shows enhanced cytotoxicity after 48-h or 72-h incubations. This result was further confirmed by optical microscopy images of HeLa cells after incubation with free DoxHCl and DoxHCl-MS42@PEG/TMS-hy-c at equivalent doxorubicin concentration (0.1 μM). Compared to the control image (only medium and serum incubation, Figure 9d), some viable cells were still observed after 48-h free DoxHCl exposure (Figure 9e), but all the HeLa cells changed to spherical or irregular morphology (damaged or dead cells) after 48-h DoxHCl-MS42@PEG/TMS-hy-c exposure (Figure 9f). The enhanced cytotoxicity of DoxHCl-MS42@PEG/TMS-hy-c is likely due to the slow drug release from DoxHCl-MS42@PEG/TMS-hy-c NPs associated or taken up by HeLa after 24-h incubation. Therefore, more localized doxorubicin was delivered to HeLa cells. In addition, the comparison of cytotoxicity of DoxHCl-MS42@PEG/TMS-hy-c and Dox-MS42@PEG/TMS-hy-c is shown in Figure 10a and 10b. Both exhibited dose- and time-dependent cytotoxicity to HeLa cells. On the basis of IC_{50} data, DoxHCl-MS42@PEG/TMS-hy-c has cytotoxic efficacy on HeLa cells higher than that of Dox-MS42@PEG/TMS-hy-c; this is likely due to faster and higher percentage of drug release from DoxHCl-MS42@PEG/TMS-hy-c NPs. Although

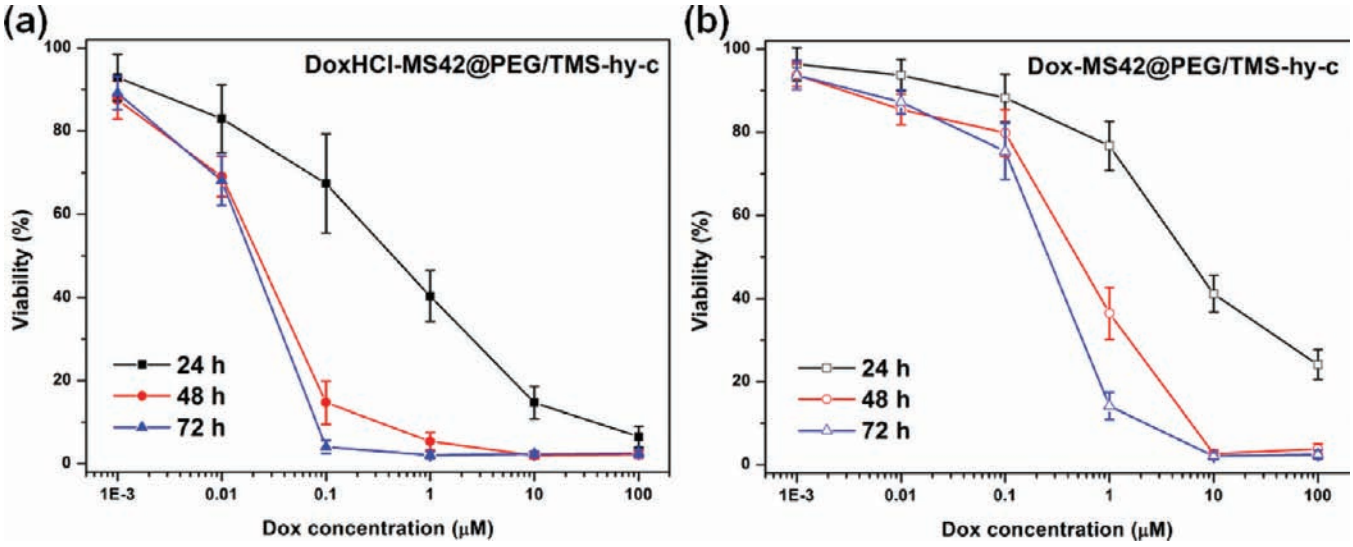

Figure 10. Cell viability of HeLa cells after different incubation times (24, 48, or 72 h) with different concentrations of (a) DoxHCl-MS42@PEG/TMS-hy-c and (b) Dox-MS42@PEG/TMS-hy-c. Data represent mean ± SD from at least three independent experiments done in triplicate.

the Dox-MS42@PEG/TMS-hy-c has lower cytotoxic efficacy, the poorly water-soluble doxorubicin is able to disperse well in aqueous solutions and kill cancer cells when delivered by MS42@PEG/TMS-hy-c. The slow release property of Dox-MS42@PEG/TMS-hy-c may be useful for cases that require long-term cancer therapy.

CONCLUSIONS

In summary, the external and internal surfaces of MS NPs were comodified with two types of organosilanes, hydrophilic silane (PEG-silane) and hydrophobic silane (TMS or TFS), accompanied by a hydrothermal treatment to increase their dispersity and long-term colloidal stability in biologically relevant media. Importantly, these highly organomodified NPs can be dried and redispersed into a buffer solution with no significant change in size or stability. To demonstrate the versatility of this hydrothermal-assisted dual-organosilane modification method, we further demonstrated the redispersity of ultrasmall (25 nm), fluorescent, and magnetic comodified MS NPs. These highly organomodified MS NPs also exhibited high biocompatibility as measured by a red blood cell lysis assay and platelet membrane integrity assay as well as unperturbed cell viability to human endothelial and skin fibroblast cells. In addition, a common anticancer drug, doxorubicin, with two different forms, water-soluble DoxHCl and poorly water-soluble Dox, were loaded into these highly organomodified MS NPs. Most importantly, these drug-loaded MS NPs can also be dried and resdispered in aqueous solution without significant hydrodynamic size change compared unloaded MS NPs; this is especially important for the poorly water-soluble Dox-loaded MS NPs. This is the first example showing the redispersity of MS NPs after drug loading. The Dox-loaded MS NPs exhibited slower drug release kinetics and lower percent Dox release compared to DoxHCl-loaded MS NPs. Finally, these redispersible drug-loaded MS NPs showed dose- and time-dependent cytotoxic effects on cancerous (HeLa) cells. The DoxHCl-loaded MS NPs further exhibited cytotoxicity higher than that of free DoxHCl. We believe that these ultrastable, redispersible, and small MS nanotherapeutics have great potential in passive tumor targeting and therapy applications.

ASSOCIATED CONTENT

Supporting Information. Additional experimental details of the reactive oxygen species (ROS) assay. Enlarged TEM images of MS42@PEG/TMS-hy-c, MS42@PEG/TMS-hy-c, and MS25@PEG/TMS-hy-c NPs. Histograms of particle size distributions of MS42-d and MS42@PEG/TMS-hy-c NPs before and after 10-day SBF aging at 37 °C. ROS generation in human endothelial cells by MS42@PEG/TMS-hy-c. This material is available free of charge via the Internet at http://pubs.acs.org.

AUTHOR INFORMATION

Corresponding Author
chaynes@umn.edu

ACKNOWLEDGMENT

This work was funded by a grant from National Science Foundation (NSF, CHE-0645041). Y.-S.L., N.A., and K.R.H. acknowledge financial support from Taiwan Merit Scholarship (NSC-095-SAF-I-564-052-TMS), Heisig/Gleysteen Chemistry Summer Research Program, and National Science Foundation Graduate Research Fellowship, respectively. The TEM and XRD measurements were carried out in the College of Science and Engineering Characterization Facility, University of Minnesota, which receives partial support from NSF through National Nanotechnology Infrastructure Network (www.mrfn.org) via the MRSEC program. We thank Professor G. Veglia and Dr. N. Traaseth for obtaining the solid-state ^{29}Si MAS NMR spectra at the University of Minnesota Nuclear Magnetic Resonance Facility.

REFERENCES

(1) Farokhzad, O. C.; Langer, R. *ACS Nano* **2009**, *3*, 16–20.
(2) Xie, J.; Lee, S.; Chen, X. *Adv. Drug Delivery Rev.* **2010**, *62*, 1064–1079.
(3) Rosenholm, J. M.; Sahlgren, C.; Lindén, M. *Nanoscale* **2010**, *2*, 1870–1883.
(4) Vivero-Escoto, J. L.; Slowing, I. I.; Trewyn, B. G.; Lin, V. S.-Y. *Small* **2010**, *6*, 1952–1967.

(5) He, Q.; Shi, J. *J. Mater. Chem.* **2011**, *21*, 5845–5855.
(6) Wu, S.-H.; Lin, Y.-S.; Hung, Y.; Chou, Y.-H.; Hsu, Y.-H.; Chang, C.; Mou, C.-Y. *ChemBioChem* **2008**, *9*, 53–57.
(7) He, Q.; Zhang, Z.; Gao, F.; Li, Y.; Shi, J. *Small* **2011**, *7*, 271–280.
(8) Huang, X.; Li, L.; Liu, T.; Hao, N.; Liu, H.; Chen, D.; Tang, F. *ACS Nano* **2011**, *5*, 5390–5399.
(9) Lin, Y.-S.; Haynes, C. L. *J. Am. Chem. Soc.* **2010**, *132*, 4834–4842.
(10) Yu, T.; Malugin, A.; Ghandehari, H. *ACS Nano* **2011**, *5*, 5717–5728.
(11) Kim, H.; Kim, S.; Park, C.; Lee, C.; Park, H. J.; Kim, C. *Adv. Mater.* **2010**, *22*, 4280–4283.
(12) Luo, Z.; Cai, K.; Hu, Y.; Zhao, L.; Liu, P.; Duan, L.; Yang, W. *Angew. Chem., Int. Ed.* **2011**, *50*, 640–643.
(13) Schlossbauer, A.; Kecht, J.; Bein, T. *Angew. Chem., Int. Ed.* **2009**, *48*, 3092–3095.
(14) Bernardos, A.; Mondragón; Aznar, E.; Marcos, M. D.; Martínez-áñez, R.; Sancenón, F.; Soto, J.; Barat, J. M.; Pérez-Payá, E.; Guillem, C.; Amorós, P. *ACS Nano* **2010**, *4*, 6353–6368.
(15) Lee, C.-H.; Cheng, S.-H.; Huang, I.-P.; Souris, J. S.; Yang, C.-S.; Mou, C.-Y.; Lo, L.-W. *Angew. Chem., Int. Ed.* **2010**, *49*, 8214–8219.
(16) Muhammad, F.; Guo, M.; Qi, W.; Sun, F.; Wang, A.; Guo, Y.; Zhu, G. *J. Am. Chem. Soc.* **2011**, *133*, 8778–8781.
(17) Rim, H. P.; Min, K. H.; Lee, H. J.; Jeong, S. Y.; Lee, S. C. *Angew. Chem., Int. Ed.* **2011**, *50*, 8853–8857.
(18) Liong, M.; Lu, J.; Kovochich, M.; Xia, T.; Ruehm, S. G.; Nel, A. E.; Tamanoi, F.; Zink, J. I. *ACS Nano* **2008**, *2*, 889–896.
(19) Wang, L.-S.; Wu, L.-C.; Lu, S.-Y.; Chang, L.-L.; Teng, I.-T.; Yang, C.-M.; Ho, J.-A. A. *ACS Nano* **2010**, *4*, 4371–4379.
(20) Meng, H.; Xue, M.; Xia, T.; Ji, Z.; Tarn, D. Y.; Zink, J. I.; Nel, A. E. *ACS Nano* **2011**, *5*, 4131–4144.
(21) Urata, C.; Yamada, H.; Wakabayashi, R.; Aoyama, Y.; Hirosawa, S.; Arai, S.; Takeoka, S.; Yamauchi, Y.; Kuroda, K. *J. Am. Chem. Soc.* **2011**, *133*, 8102–8105.
(22) Cauda, V.; Argyo, C.; Piercey, D. G.; Bein, T. *J. Am. Chem. Soc.* **2011**, *133*, 6484–6486.
(23) Lin, Y.-S.; Abadeer, N.; Haynes, C. L. *Chem. Commun.* **2011**, *47*, 532–534.
(24) Kokubo, T.; Kushitani, H.; Sakka, S.; Kisugi, T.; Yamamuro, T. *J. Biomed. Mater. Res.* **1990**, *24*, 721–734.
(25) Lin, Y.-S.; Haynes, C. L. *Chem. Mater.* **2009**, *21*, 3979–3986.
(26) Coradin, T.; Eglin, D.; Livage, J. *J. Spectrosc.* **2004**, *18*, 567–576.
(27) Liao, K.-H; Lin, Y.-S.; Macosko, C. W.; Haynes, C. L. *ACS Appl. Mater. Interfaces* **2011**, *3*, 2607–2615.
(28) Ge, S.; Woo, E.; White, J. G.; Haynes, C. L. *Anal. Chem.* **2011**, *83*, 2598–2604.
(29) He, Q.; Shi, J.; Zhu, M.; Chen, Y.; Chen, F. *Microporous Mesoporous Mater.* **2010**, *131*, 314–320.
(30) Koyano, K. A.; Tatsumi, T.; Tanaka, Y.; Nakata, S. *J. Phys. Chem. B* **1997**, *101*, 9436–9440.
(31) Cauda, V.; Schlossbauer, A.; Bein, T. *Microporous Mesoporous Mater.* **2010**, *132*, 60–71.
(32) Kim, D.; Lin, Y.-S.; Haynes, C. L. *Anal. Chem.* **2011**, *83*, 8377–8382.
(33) Lin, Y.-S.; Tsai, C.-P.; Huang, H.-Y.; Kuo, C.-T.; Hung, Y.; Huang, D.-M.; Chen, Y.-C.; Mou, C.-Y. *Chem. Mater.* **2005**, *17*, 4570–4573.
(34) Chen, Y.; Chen, H.; Zeng, D.; Tian, Y.; Chen, F.; Feng, J.; Shi, J. *ACS Nano* **2010**, *4*, 6001–6013.
(35) Zhu, Y.; Ikoma, T.; Hanagata, N.; Kaskel, S. *Small* **2010**, *6*, 471–478.